

Rotational Stability Index (RSI) point: postural stability in planar bipeds

Goswami Dip* and Vadakkepat Prahlad

Department of Electrical and Computer Engineering, National University of Singapore, 4 Engineering Drive 3, Singapore 117576. E-mail: prahlad@ieee.org

(Received in Final Form: September 15, 2010)

SUMMARY

The postural stability of bipedal robots is investigated in perspective of foot-rotation during locomotion. With foot already rotated, the biped is modeled as an underactuated kinematic structure. The stability of such biped robots is analyzed by introducing the concept of *rotational stability*. The *rotational stability* investigates whether a biped would lead to a flat-foot posture or the biped would topple over. The *rotational stability* is quantified as a ground reference point named “rotational stability index (RSI)” point. Conditions are established to achieve *rotational stability* during biped locomotion using the concept of the RSI point. The applicability of the RSI point is illustrated through experimentation for the landing stability analysis of the bipedal jumping gaits.

The traditional stability criteria such as zero-moment point (ZMP) [M. Vukobratovic and B. Borovac, “Zero-moment point – thirty five years of its life,” *Int. J. Humanoid Robot.* 1(1), 157–173 (2004)] and foot-rotation indicator (FRI) [A. Goswami, “Postural stability of biped robots and the foot-rotation indicator (FRI) point,” *Int. J. Robot. Res.* 18(6), 523–533 (1999)] are not applicable to analyze biped’s postural stability when foot is already rotated. The RSI point is established as a stability criteria for planar bipedal locomotion in presence of foot rotation.

KEYWORDS: Internal dynamics; *Rotational stability*; Rotational-stability index (RSI) point.

1. Introduction

Postural stability of biped locomotion has been in the research focus for the past few decades. The term “postural stability” during various bipedal activities refers to maintaining balance to keep the biped upright. Postural stability is broadly classified into static and dynamic stabilities. The biped is always stable when the locomotion is statically stable. Dynamically stable gait has certain unstable phases.

Zero-moment point (ZMP) is a widely used concept to analyze postural stability of legged systems.¹² The ZMP is the point on the ground where the horizontal component of

the resultant of moments acting on the legged system is zero. To maintain postural stability in legged systems, the ZMP is kept within the area covered by the foot, i.e., the support polygon.^{13–15} Biped locomotion is normally considered with flat foot while utilizing the ZMP-based stability criterion.^{14,15}

The ZMP criterion is not applicable to point foot bipeds.^{16–19} The absolute orientation of the biped is considered as an additional passive degree of freedom (DOF) in point foot bipeds. The concepts of periodicity and orbital stability are useful while dealing with the associated stability issues.^{18–20} By periodically attaining certain postures, even though statically unstable, orbital stability is achievable. The concept of orbital stability is applicable to periodic gaits, such as walking, running, and hopping,⁵ and not suitable for stability analysis of aperiodic gaits, such as jumping.

In various gaits for bipeds with nontrivial foot size, one fundamental consideration is the possibility of rotation of the overall biped about the foot edge. Such foot rotation depends on biped’s “rotational equilibrium”.^{1,4} Foot rotation is an important aspect to look into while addressing stable locomotion. The foot-rotation indicator (FRI) point explains the occurrence of foot rotation.¹ If the FRI point is outside the foot-print area, the foot rotates about certain point on the foot boundary. The foot rotation changes the absolute orientation of the biped bringing in a passive DOF, which makes the bipedal systems *underactuated*. Foot/feet rotation can occur both in single-support phase and in double-support phase [Figs. 1(a) and (b)].

The ground reference points such as ZMP and FRI use ground reaction force (GRF) for their evaluation. The locations of such ground reference points depend on the distribution of GRF at the foot–ground contact surface. When foot is rotated, GRF acts on the point about which the foot is rotating. ZMP/FRI fails to indicate the stability aspects in such situations. Hence, foot rotation is often noted to reflect a loss of stability in biped locomotion and is dealt by preventing foot rotation.^{1,2,6}

Foot rotation during locomotion does not essentially indicate postural imbalance of the biped. The biped can still be stable even in the presence of foot rotation. The configuration, when foot is rotated about the edge, is commonly referred as tiptoe configuration [Figs. 1(a)–(c)].

* Corresponding author. E-mail: dip.goswami@ieee.org

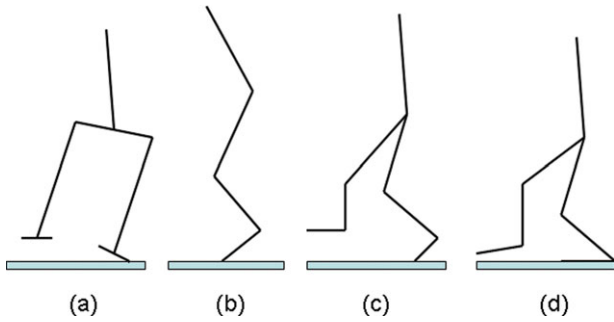


Fig. 1. (a) Foot rotation in frontal plane; (b) foot rotation in double-support phase (sagittal plane); (c) foot rotation in single-support phase (sagittal plane); (d) foot rotation in swinging leg (sagittal plane).

The biped with rotated foot often becomes *underactuated*. In some scenarios, the biped is fully actuated even in the presence of foot rotation [e.g., Fig. 1(d)]—foot rotation occurs in swinging leg]. Postural stability of fully actuated bipeds is commonly analyzed by the ZMP or FRI criterion.^{1,14,15,22} However, such analysis techniques are not suitable for stability analysis of underactuated bipeds.

The postural stability of underactuated bipedal model is investigated in ref. [3] while analyzing the landing stability of bipedal jumping gaits. While considering the foot rotation about toe, e.g., Figs. 1(b) and (c), the foot rotates back to flat-foot posture, depending on the values of “critical kinetic index” and “critical potential index,” which further depend on the controller design.

In this research, a novel stability concept *rotational stability* is introduced to analyze the stability in the underactuated bipeds with foot rotation. The rotational stability investigates whether the biped would lead to a flat-foot posture from an underactuated configuration with foot rotation. A ground reference point “rotational-stability index (RSI)” point is proposed to measure the degree of *rotational stability*. The location of the RSI point depends both on the bipedal dynamic parameter and on the controller design parameter. Conditions are established based on the RSI point to analyze postural stability during bipedal locomotion and are validated by investigating the landing stability of jumping gaits of a biped. While the stability analysis in ref. [3] is restricted to the associated stability aspects of foot rotation about toe, the RSI point-based stability criterion explains the foot rotation about both the toe and heel. Moreover, one needs to compute *critical kinetic index* and *critical potential index* offline in order to verify the rotational stability of a particular bipedal gait. On the other hand, the proposed RSI point is utilized as an online stability criterion for discrete-time control implementation.

Section 2 describes the planar biped model, the computation of the associated dynamics, and the control architecture. The concepts of *rotational stability* and RSI point are introduced in Section 3. Section 4 explains the RSI point-based criterion to analyze stability in bipedal locomotion. Simulations and experimentations on bipedal jumping gaits are described in Section 5, and conclusions are drawn in Section 6.

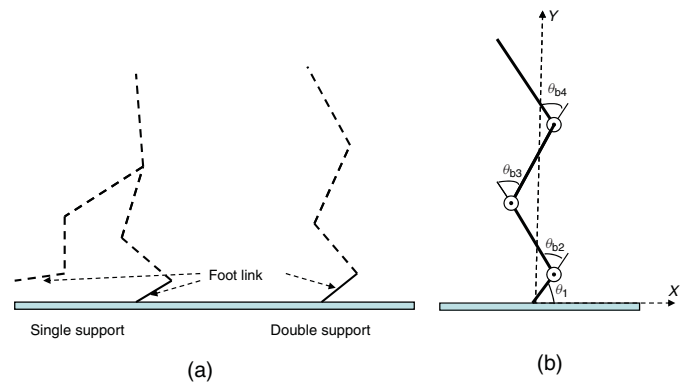


Fig. 2. (a) Planar bipeds with foot rotation (b) biped model.

2. Planar Biped Model and Control Architecture

Foot-rotation during locomotion may occur in both single-support and double-support phases [Fig. 2(a)]. With foot rotation, an unactuated DOF appears at the joint between the foot and the ground. Let θ_1 is the absolute angle between the foot and the ground [Fig. 2(b)]. The number of actuated DOF depends on the biped’s structure and let the vector of the body’s actuated joint angular coordinates be θ_b . For example, $\theta_b = [\theta_{b2} \theta_{b3} \theta_{b4}]^T$ in Fig. 2(b). Biped’s absolute orientation is indicated by the generalized coordinates $\theta_a = [\theta_1 \theta_b^T]^T$. The Cartesian coordinate of the toe (joint between the foot and ground) is indicated by (x_0, y_0) and vector of all of other joint’s Cartesian coordinates is (x_b^T, y_b^T) .

2.1. Dynamics

While considering foot rotation during locomotion, the biped’s dynamic model is obtained using the Lagrangian formulation.¹⁰ The biped with n links in presence of foot rotation (Fig. 2) has dynamics with the following form:

$$M(\theta_b)\ddot{\theta}_a + V(\theta_a, \dot{\theta}_a) + G(\theta_a) = \tau_s, \quad (1)$$

where M is the $n \times n$ inertial matrix about toe, V is an $n \times 1$ vector containing the Coriolis and centrifugal terms, and G is the $n \times 1$ gravity vector. τ_s is the vector of the generalized forces and torques applied to the biped

$$\tau_s = [0 \ \tau_2 \ \tau_3 \ \dots \ \tau_n]^T. \quad (2)$$

And $u_s = [\tau_2 \ \tau_3 \ \dots \ \tau_n]^T$ are the torques applied by the various joint actuators. The body’s joint angular positions $\theta_b = [\theta_2 \ \theta_3 \ \dots \ \theta_n]^T$.

2.2. Internal dynamics

The control input u_s is chosen using various control design techniques (e.g., *input-output linearization*⁹ or *output-zeroing technique*).⁸ Various bipedal gaits or desired θ_b can be realized/achieved by proper choice of u_s . However, the first row of (1) (due to the unactuated joint at the toe) results in an “unobservable” dynamics shown in (3).¹ This is known as *internal dynamics* of the system. The postural stability of

¹ $M_{r,c}$ indicates the element in the r th row and c th column of the inertia matrix M .

biped structure with rotated foot is governed by the system's internal dynamics.

$$M_{11}(\theta_b)\ddot{\theta}_1 + \sum_{i=2}^n M_{1i}(\theta_b)\ddot{\theta}_i + \sum_{i=2}^n V_i(\dot{\theta}_1, \dot{\theta}_b)\dot{\theta}_i + G_1(\theta_1, \theta_b) = 0. \quad (3)$$

The internal dynamics in (3) can be transformed into a form, as shown in (4).¹⁹

$$\begin{aligned} \dot{\theta}_1 &= \frac{1}{M_{11}(\theta_b)}\sigma - \sum_{i=2}^n \frac{M_{1i}(\theta_b)}{M_{11}(\theta_b)}\dot{\theta}_i, \\ \dot{\sigma} &= mgx_{cm}(\theta_a), \end{aligned} \quad (4)$$

where σ is the angular momentum about the biped's toe, m is the total mass of the biped, g is the gravitational acceleration, and $x_{cm}(\theta_a)$ is the ground projection of the biped's center of mass (CM). In (4), $\theta_1 > 0$ indicates forward foot rotation and $\theta_1 < 0$ when the foot rotates about the other end of the foot (other than toe). The boundedness of the internal dynamics is essential for the postural stability of the biped.

2.3. Control architecture and system analysis

The state vector of the bipedal dynamics (1) can be chosen as $x_s := (\theta_1, \sigma, x_b)^T$, where $x_b := (\theta_b^T, \dot{\theta}_b^T)^T$. Therefore, the bipedal dynamics (1) is expressed as a combination of (5)–(7).

$$\dot{\theta}_1 = \frac{1}{M_{11}(\theta_b)}\sigma - \frac{1}{M_{11}(\theta_b)} \sum_{i=2}^n M_{1i}(\theta_b)\dot{\theta}_i, \quad (5)$$

$$\dot{\sigma} = mgx_{cm}(\theta_a), \quad (6)$$

$$\begin{aligned} \dot{x}_b &= \begin{bmatrix} \dot{\theta}_b \\ \text{inv}(M)_{2-n}(-V - G) \end{bmatrix} + \begin{bmatrix} 0 \\ \text{inv}(M)_{2-n}\tau_s \end{bmatrix} \\ &= f_b(x_s) + g_b(x_s)u_s, \end{aligned} \quad (7)$$

where $\text{inv}(\cdot)$ returns the inverse of a matrix and $\text{inv}(M)_{i-j}$ indicates the matrix consisting of the elements from i th to j th rows of the inverse matrix of M .

In the equivalent two-link model⁷ of the biped (Fig. 3), the foot link acts as one link and the distance from the ankle to the CM of the rest of the biped acts as another link. The Cartesian coordinate $(x_{cm0}(\theta_b), y_{cm0}(\theta_b))$ is as per Fig. 3 [with respect to the coordinate system (X_f, Y_f)].

Let us define

$$\begin{aligned} K_1(x_b) &= \frac{1}{M_{1,1}(\theta_b)} \text{kg}^{-1} \text{m}^{-2}, \\ K_2(x_b) &= mg\sqrt{x_{cm0}^2(\theta_b) + y_{cm0}^2(\theta_b)} \text{Nm}, \\ K_3(x_b) &= \tan^{-1}\left(\frac{x_{cm0}(\theta_b)}{y_{cm0}(\theta_b)}\right) \text{rad}, \\ K_4(x_b) &= \sum_{i=2}^n M_{1i}(\theta_b)\dot{\theta}_i \text{kg m}^2 \text{s}^{-1}. \end{aligned} \quad (8)$$

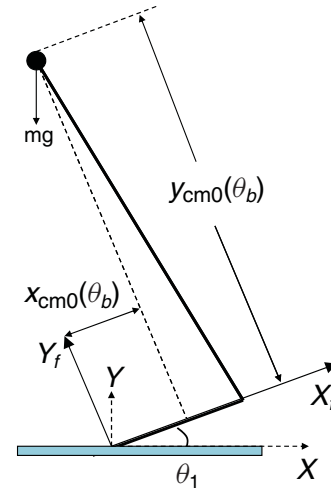


Fig. 3. Two-link equivalent model of the biped with foot.

The Eqs. (5)–(7) then can be rewritten as (9).

$$\begin{aligned} \dot{\theta}_1 &= K_1(x_b)\sigma - K_1(x_b)K_4(x_b), \\ \dot{\sigma} &= K_2(x_b)\sin(\theta_1 - K_3(x_b)), \\ \dot{x}_b &= f_b(x_s) + g_b(x_s)u_s. \end{aligned} \quad (9)$$

2.4. Control implementation and discretization

The control law u_s is typically implemented on an embedded processor by sampling (with sampling interval t_s) the states at time instants $t_k = k * t_s, k \in [0, 1, 2, \dots]$ and updating the actuator values. Thereafter, $u_s(t) = F(x_s(t_k))$ are computed and provided at the joint actuators. Hence, the input value u_s is held constant in between two consecutive samples, i.e., $u_s(t) = F(x_s(t_k))$ for $t \in [t_k, t_{k+1}]$. The overall system behaves as a discrete-time system as per (10) and (11). $\Lambda_1(\cdot)$ and $\Lambda_2(\cdot)$ are the discrete-time equivalents of the system (9)². Usually, u_s is designed assuming that the sampling time t_s is small enough for (11) to be considered as (7). With proper choice of u_s , it is possible to realize certain bipedal gaits such as walking and jumping. However, boundedness of $(\theta_1(t_k), \sigma(t_k))$ is essential for the postural stability of a particular gaits. In the following sections, such stability aspects are addressed.

$$\begin{bmatrix} \theta_1(t_{k+1}) \\ \sigma(t_{k+1}) \end{bmatrix} = \Lambda_1(\theta_1(t_k), \sigma(t_k), K_i(x_b(t_k))), \quad (10)$$

$$x_b(t_{k+1}) = \Lambda_2(f_b(x_s(t_k)), g_b(x_s(t_k)), u_s(x_s(t_k))), \quad (11)$$

where $i \in [1, 2, 3, 4]$.

3. Rotational Stability

During biped locomotion, foot rotation may occur both in forward and in backward directions. The foot-rotation essentially results in tiptoed bipedal configuration. While

² $\Lambda_1(\cdot)$ and $\Lambda_2(\cdot)$ can be the solution of numerical integration methods such as Runge–Kutta fourth order.

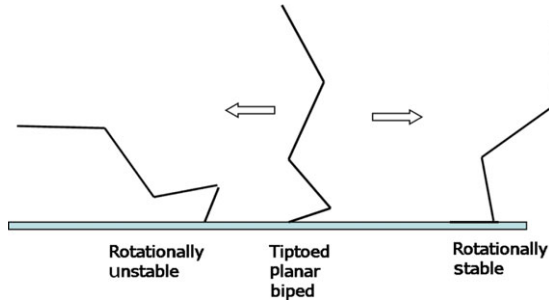


Fig. 4. Rotational Stability.

the biped is in motion, such tiptoeed configurations can lead to either a flat-foot posture or toppling over of the biped. In various bipedal gaits, such as jumping, hopping, and running, the stability of the overall structure is governed by its possibility to achieve flat foot from a tiptoeed posture. For example, the landing process of jumping gaits is stable when the gait ensures that the biped achieves flat-foot posture with time.³ The reachability of flat-foot posture is important in bipedal gaits, because margin of postural stability is more in flat-foot bipeds, and such stability margin can be analyzed using ZMP/FRI/FZMP.^{1,2}

A term *rotational stability* is introduced to formally analyze the possibility of the bipedal gaits to achieve a flat-foot posture from a tiptoeed configuration.

Definition 1: (Rotational Stability) A biped is “rotationally stable” if its dynamics leads to a flat-foot posture with time.

Physical significance of the *rotational stability* is explained in Fig. 4. The biped leads to a flat-foot posture when it is *rotationally stable* and topples over when it is not. In other words, a biped is rotationally stable if $\theta_1(t_k)$ in (10) reaches $\theta_1 = 0$ plane with time. In biped locomotion, the presence of foot rotation is often indicated as postural instability.^{1,2,6} The novelty of the concept – *rotational stability* – lies in its applicability to explain stability aspects when the foot is already rotated³.

3.1. Rotational stability and rotational stability index point

The internal dynamics of planar bipedal structures with foot rotation is shown in Section 2. It is noticed that the biped leads to a flat-foot posture if the solution vector of (10) and (11) reaches the $\theta_1(t_k) = 0$ plane, which is also required to achieve rotational stability. In this section, we illustrate how to achieve rotational stability by achieving boundedness of the internal dynamics.

The choice of control input u_s should ensure that the discrete-time system in (10) reaches $\theta_1(t_k) = 0$ plane to achieve rotational stability. The control input u_s and the actuator updates x_b are held constant in between two consecutive samples, i.e., $u_s(t) = F(x_s(t_k))$ and $x_b(t) = x_b(t_k)$ ⁴ for $t \in [t_k, t_{k+1}]$. Therefore, the biped's internal

³ The postural stability is associated with the act of keeping the bipedal structure upright. The postural stability in the presence of foot rotation is explained utilizing the concept of rotational stability.

⁴ The presented analysis in Lemmas 1 and 2 evaluates certain stability aspects of the biped at $t = t_k$. Hence, the computation is performed with $x_b(t) = x_b(t_k)$.

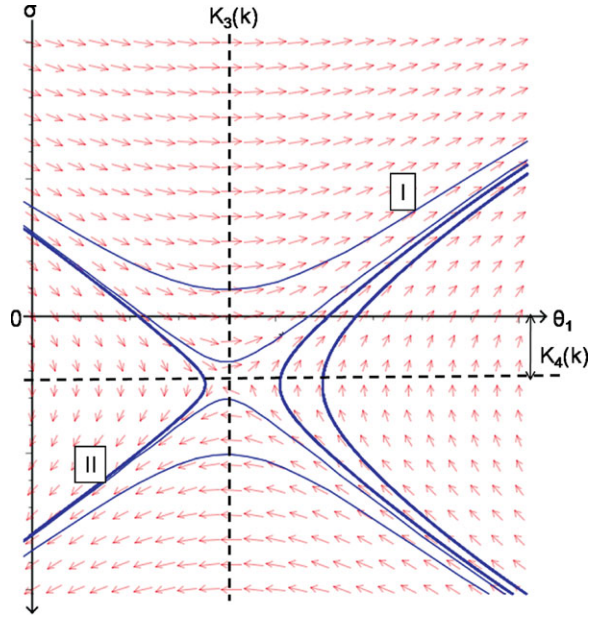


Fig. 5. State-space portrait of (12). Trajectory I: Member of the set of trajectories going out with increasing θ_1 . Trajectory II: Member of the set of trajectories reaching the $\theta_1 = 0$ plane.

dynamics shown in (4) becomes as per (12) in any time interval $t \in [t_k, t_{k+1}]$ in between two consecutive samples.

$$\begin{aligned}\dot{\theta}_1 &= K_1(k)\sigma - K_1(k)K_4(k), \\ \dot{\sigma} &= K_2(k)\sin(\theta_1 - K_3(k)),\end{aligned}\quad (12)$$

where $K_i(k) = K_i(x_b(t_k))$ for $i \in [1, 2, 3, 4]$ are constants. The initial conditions of (12) are $\theta_{10} = \theta_1(t_k)$ and $\sigma_0 = \sigma(t_k)$.

The internal dynamics (12) has one equilibrium point at $(\theta_1, \sigma) = (K_3(k), K_4(k))$ for $0 < \theta_1 < \pi$. The nature of the equilibrium point is indicated in the state-space portrait in Fig. 5. It can be noticed that the equilibrium point is a *saddle point* and unstable (by linearization and applying *Lyapunov's indirect method*).¹¹ In Fig. 5, one set of trajectories are going away with increasing θ_1 (Trajectory I) and another set of trajectories are approaching $\theta_1 = 0$ plane (Trajectory II). How the various parameters in (12) affect these trajectories is given by Lemma 1.

Lemma 1: Consider the continuous-time system (12) defined in any time interval $t \in [t_k, t_{k+1}]$ with initial conditions $\theta_{10} = \theta_1(t_k) > 0$ and $\sigma_0 = \sigma(t_k)$. The solution vector (θ_1, σ) of (12) from initial condition (θ_{10}, σ_0) reaches $\theta_1 = 0$ plane if either statement (A) or (B) is true.

- (A) $K_3(k) > \theta_{10}$ and $\sigma_0 < K_4(k) + \sqrt{\frac{2K_2(k)}{K_1(k)}(1 - \cos(\theta_{10} - K_3(k)))}$,
 (B) $K_3(k) \leq \theta_{10}$ and $\sigma_0 < K_4(k) - \sqrt{\frac{2K_2(k)}{K_1(k)}(1 - \cos(\theta_{10} - K_3(k)))}$.

Proof: Provided in Appendix A.

Definition 2: (RSI Point) Consider a biped with respect to the world coordinate X - Y , and origin being located at the toe of the rotated foot (Fig. 2). The internal dynamics of the biped defined in any time interval $t \in [t_k, t_{k+1}]$ with

initial conditions $\theta_{10} = \theta_1(t_k) > 0$ and $\sigma_0 = \sigma(t_k)$ is shown in (12). The RSI point is defined as a point on the ground ($x_{\text{RSI}}(t_k), y_{\text{RSI}}(t_k) = 0$) as per (13).

$$x_{\text{RSI}}(t_k) = x_{\text{cm}}(\theta_{10}, \theta_b(t_k)) - \frac{\sigma_0 - K_4(k)}{mg} \sqrt{\frac{K_1(k)K_2(k)(1 + \cos(K_3(k) - \theta_{10}))}{2}}. \quad (13)$$

Lemma 2: Consider a biped with respect to the world coordinate X - Y , and origin being located at the toe of the rotated foot (Fig. 2). The internal dynamics of the biped defined in any time interval $t \in [t_k, t_{k+1}]$ with initial conditions $\theta_{10} = \theta_1(t_k) > 0$ and $\sigma_0 = \sigma(t_k)$ is shown in (12), and the RSI point is as per Definition 2. Either statement (A) or (B) in Lemma 1 is true if $x_{\text{RSI}}(t_k) > 0$.

Proof: Provided in Appendix B.

Theorem 1: Consider a biped with respect to the world coordinates X - Y , and origin being located at the toe of the rotated foot (Fig. 2). The biped internal dynamics is (10), and the RSI point is as per Definition 2. The states $S_N = \{\theta_1(t_N), \sigma(t_N) : \theta_1(t_N) = 0\}$ are *reachable* from any given initial states $S_0 = \{\theta_{10}, \sigma_0\}$ with $\theta_{10} > 0$, if $S_0 \subset M_0$, where M_k is defined recursively by (14) for $k \in [0, 1, 2, \dots, N]$.

$$M_k = \{\theta_1(t_k), \sigma(t_k) : x_{\text{RSI}}(t_k) > 0, \Lambda_1(\theta_1(t_k), \sigma(t_k), K_i(x_b(t_k))) \in M_{k+1}\}. \quad (14)$$

Proof: We prove Theorem 1 by applying the concept of minimax reachability.²³ The states $S_N = \{\theta_1(t_N), \sigma(t_N) : \theta_1(t_N) = 0\}$ is the target set, and the reachability of S_N from S_0 is analyzed. It is easily seen from the recursive Eq. (14), if $S_0 \subset M_0$, then $S_k \subset M_k$ for all k . Therefore, $x_{\text{RSI}}(t_k) > 0$ for all k . From Lemmas 1 and 2, we can say that $S_N = \{\theta_1(t_N), \sigma(t_N) : \theta_1(t_N) = 0\}$ is reachable, if $x_{\text{RSI}}(t_{N-1}) > 0$, which is true if $S_0 \subset M_0$. Hence, the states $S_N = \{\theta_1(t_N), \sigma(t_N) : \theta_1(t_N) = 0\}$ are *reachable* from any given initial states $S_0 = \{\theta_{10}, \sigma_0\}$, if $S_0 \subset M_0$.

Proposition 1: A bipedal structure with dynamics represented by (10) and (11) is rotationally stable if $x_{\text{RSI}}(t_k) > 0$ for all k .

Proof: It is clear from Theorem 1 and (14) that the biped dynamics represented by (10) and (11) reaches $\theta_1(t_k) = 0$ plane, if $x_{\text{RSI}}(t_k) > 0$ for all k .

It is notable from Lemmas 1 and 2 that $x_{\text{RSI}}(t_k) > 0$ at $t = t_k$ indicates that the biped will lead to a flat-foot posture with time if $x_b(t) = x_b(t_k)$. However, $x_b(t)$ is not constant in the interval $[t_k, t_{k+1}]$ and vary according to (9). Therefore, there is a need to compute $x_{\text{RSI}}(t_{k+1})$ at sampling instant $t = t_{k+1}$. As $x_b(t)$ is not constant, $x_b(t) = x_b(t_{k+1})$ while computing $x_{\text{RSI}}(t_{k+1})$. $x_{\text{RSI}}(t_{k+1}) > 0$ indicates that the biped will have a flat-foot posture, if $x_b(t) = x_b(t_{k+1})$. Similarly, RSI point is computed at every sampling instant. The biped is rotationally stable only if $x_{\text{RSI}}(t_k) > 0$ for all k or $x_{\text{RSI}}(t) > 0$ for all samples. Proposition 1 states the above aspect of the bipedal stability. The proposed RSI point can be utilized as a constraint on controller design. The controller must be

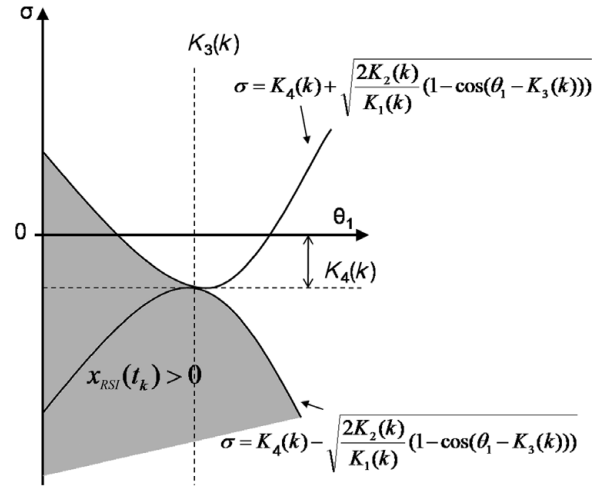


Fig. 6. RSI point and state-space portrait.

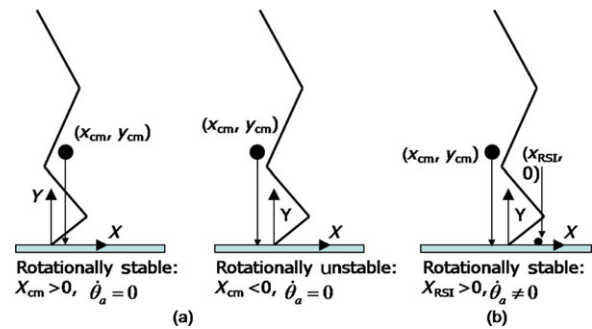


Fig. 7. Rotational Stability.

designed in such a way that closed-loop dynamics satisfies the RSI-based stability criterion stated in Proposition 1.

3.2. Notes on the RSI point

Rotationally stable postures: The two loci for $\sigma = K_4(k) + \sqrt{\frac{2K_2(k)}{K_1(k)}(1 - \cos(\theta_{10} - K_3(k)))}$ and $\sigma = K_4(k) - \sqrt{\frac{2K_2(k)}{K_1(k)}(1 - \cos(\theta_{10} - K_3(k)))}$ are shown in Fig. 6. $x_{\text{RSI}}(t_k) > 0$ in any bipedal posture corresponding to the shaded area in Fig. 6. Hence, the shaded area corresponds to *rotationally stable* postures.

Rotational stability in stationary bipeds: Consider the expression of $x_{\text{RSI}}(t_k)$ in (13). If $\sigma_0 = 0$ and $\dot{\theta}_b = 0$ in (13), the stability condition in Proposition 1 effectively leads to $x_{\text{cm}}(\theta_{10}, \theta_b(t_k)) > 0$ [Fig. 7(a)]. Basically, this is the ground projection of CM (GCM) condition for stationary bipeds.¹ It is possible to explain *rotational stability* in stationary bipeds by utilizing the GCM condition. The location of RSI point addresses the effects of the nonzero joint angular velocities, i.e., $\dot{\theta}_a \neq 0$, on *rotational stability*.

Degree of rotational stability: The magnitude of the positive $x_{\text{RSI}}(t_k)$ indicates the degree of *rotational stability*. When $(\sigma_0 - K_4(k)) > 0$, larger value of $(\sigma_0 - K_4(k))$ lessen the positive magnitude of $x_{\text{RSI}}(t_k)$, leading to lesser margin of *rotational stability*. The positive value of $(\sigma_0 - K_4(k))$ signifies that counterclockwise moment is acting on the biped-inducing tendency to topple forward. Such counterclockwise moment lessens the value of

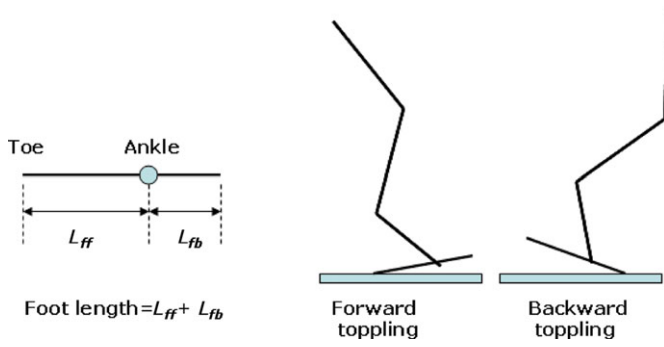


Fig. 8. Forward and backward foot rotations.

$x_{\text{RSI}}(t_k)$, indicating that the biped has lesser margin of *rotational stability*. Similar explanation is possible when $x(\theta_a) < 0$ and the biped is *rotationally stable* because the negative value of $(\sigma_0 - K_4(k))$ is such that $x_{\text{RSI}}(t_k) > 0$ [Fig. 7(b)]. The biped becomes “rotationally unstable” when $x_{\text{RSI}}(t_k) \neq 0$.

4. RSI Point-Based Stability Criteria

It is seen in Section 3.1 that RSI point can be utilized to quantify rotational stability of bipedal gaits with forward foot rotation. The idea of RSI point can further be extended for analyzing rotational stability with backward foot rotation. Moreover, the stability criteria for forward and backward foot rotation can be combined to get an overall stability criteria. In this section, we illustrate how the RSI point-based criteria for forward foot rotation is extended to establish the overall bipedal stability criterion.

Consider the foot link shown in Fig. 8. To decide on the forward toppling, we can use the criterion mentioned in *Proposition 1* with foot length $d_1 = L_{ff}$ in (1). During backward toppling, the biped rotates about the end point (other than toe) of the foot-link and can be considered like tiptoed biped about the other end point of the foot-link. In case of backward foot rotation, $\theta_1 < 0$ and the phase-portrait is the mirror image of Fig. 5. The expression for RSI with respect to the point of rotation during backward foot rotation ($x_{\text{RSI}}^b(t)$) is given by (15), where σ'_0 is the angular momentum about the point of rotation in backward direction and $K'_1(k)$, $K'_2(k)$, $K'_3(k)$, and $K'_4(k)$ are computed from (8) with foot length $d_1 = L_{fb}$.

The condition for *rotational stability* is $x_{\text{RSI}}^b(t_k) < 0$, $\forall k$ (similar to the criterion in *Proposition 1*). The relative position between $x_{\text{RSI}}^b(t_k)$ and $x_{\text{RSI}}(t_k)$ with respect to (X, Y) is given by (15).

$$x_{\text{RSI}}^b(t_k) = x_{\text{cm}}(\theta_{10}, \theta_b(t_k)) - (L_{ff} + L_{fb}) - \frac{\sigma'_0 - K'_4(k)}{mg} \times \sqrt{\frac{K'_1(k)K'_2(k)(1 + \cos(K'_3(k) - \theta_{10}))}{2}},$$

$$\implies x_{\text{RSI}}^b(t_k) = x_{\text{RSI}}(t_k) - (L_{ff} + L_{fb}). \quad (15)$$

Rotational Stability Index (RSI) point

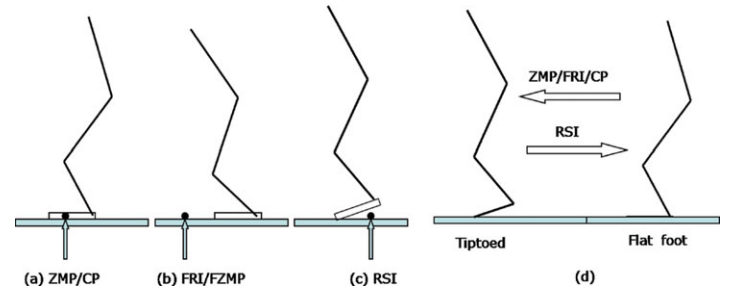


Fig. 9. ZMP/FRI/CP/FZMP and RSI: (a) foot is not going to rotate; (b) foot is about to rotate; (c) foot is rotated, and the biped is *rotationally stable*; (d) ZMP/CP/FRI indicates whether the foot is about to rotate or not, RSI point indicates whether the biped will lead to a flat-foot posture or not.

Hence, the condition to avoid backward toppling as per (16) for all k .

$$x_{\text{RSI}}^b(t_k) < 0 \implies x_{\text{RSI}}(t_k) < (L_{ff} + L_{fb}),$$

$$\implies x_{\text{RSI}}(t_k) < \text{foot length}. \quad (16)$$

4.1. Stability criterion

Merging the conditions for both forward (*Proposition 1*) and backward foot rotations in (16), the overall bipedal stability condition is rewritten as (17). It is notable for the computation of $x_{\text{RSI}}(t_k)$ that the constants in (8) is dependent on the point of foot rotation during biped locomotion. Moreover, the angular momentum σ in the expression of $x_{\text{RSI}}(t_k)$ is computed about the point of foot rotation in forward or backward directions.

$$\text{Biped stability criteria : } 0 < x_{\text{RSI}}(t_k) < \text{foot length}, \quad \forall k. \quad (17)$$

The biped will have a flat-foot posture if stability criterion (17) is satisfied at every sampling instant. Once the flat-foot posture is achieved, biped can experience an impact²¹ while the foot link touches the ground surface. Due to the impact, there is a possibility that the biped either goes into a flight phase or the foot link is again rotated in forward or backward direction. If the foot link rotates in forward or backward direction, the criterion (17) can be applied to analyze rotational stability. Although the rotational stability criterion (17) is not applicable for the flight phases, the rotational stability can again be analyzed once the biped lands on ground surface after the flight phase. Therefore, the stability criterion (17) should hold at all sampling instants whenever the biped is in touch with the ground surface and the foot link is rotated.

4.2. Comparison with other ground reference points

The RSI-based stability criterion fundamentally differs from the well-known ground reference points in a number of ways. When ZMP is within the support polygon, it coincides with the center of pressure (CP).¹ Postures with ZMP/CP within the support polygon are statically stable, and there is no foot rotation [Fig. 9(a)]. When ZMP is outside the support polygon, it is termed as Fictitious ZMP (FZMP).² The location of ZMP/FZMP being outside the support

polygon indicates that the foot is about to rotate [Fig. 9(b)]. FZMP and FRI indicate similar stability aspects of biped locomotion.² The location of FRI point indicates whether the foot is going to rotate or not. When FRI is located within the support polygon, it coincides with the ZMP. All these ground reference points investigate certain stability aspects associated with the flat-foot bipeds. Applicability of ZMP/FRI/FZMP-based stability analysis is restricted to the flat-foot bipedal locomotion. On the contrary, RSI point deals with situations when foot is already rotated, but the biped has not fallen down. The location of the RSI point indicates whether the biped is leading to a flat-foot posture or topple over [Figs. 9(c) and (d)].

In flat-foot postures, the ZMP and FRI points are computed based on the torque generated at the toe–ground contact point due to GRF. Such torques due to GRF become zero in tiptoed bipeds, because GRF acts at the point of rotation. Therefore, ZMP and FRI are not applicable for postural stability analysis when the foot is already rotated. On the other hand, the RSI point does not use GRF in its computation and is able to analyze rotational stability in tiptoed bipeds. However, the RSI point is not relevant in flat-foot postures. The torques due to GRF will appear in Eqs. (3) and (4) in flat-foot bipeds. Therefore, the stability concepts associated with RSI and ZMP/FRI are complementary.

5. Simulations and Experiments

The applicability of the RSI point in stability analysis of biped locomotion is illustrated by simulation and experimental validation on the landing stability associated with bipedal jumping gaits.³ We use similar simulation and experimental setup as described in ref. [3]. During the landing phase of the jumping gaits, the biped lands on toe with foot already rotated. The biped either lands stably or topple forward depending on the rotational stability of such landing dynamics. We limit our study to forward toppling, as backward toppling can be performed in a similar way. Simulation studies and experimental verifications are performed on the bipedal platform, Bio-Robotics Activities in Locomotion 2.0 (BRAIL 2.0). The biped robot—BRAIL 2.0—is described in Section 5.1. The parameters of the BRAIL 2.0 biped are shown in Table I.

5.1. The biped: BRAIL 2.0

BRAIL 2.0 is a 6-DOF two-legged robot. Each leg has three links: foot, shank, and thigh. The free end of the foot link is the toe. The joint between the foot link and the shank link is the ankle. The joint between the shank link and the thigh



Fig. 10. BRAIL 2.0 and Autodesk design.

link is the knee, while that between the two thigh links of the legs is the hip. Each leg has three joints, and each joint has one actuator. The link attached at the hip is the torso link. A weight is attached at the distal end of the torso link. The amount and location of the weight on the torso link are adjustable. The biped has a total of seven links. BRAIL 2.0 cannot bend in frontal plane as it does not have any “roll” DOF in its legs. BRAIL’s motion is restricted to sagittal plane, making it a planar robot.

The mechanical design is done in Autodesk Inventor (usa.autodesk.com). The Autodesk design and the robot BRAIL 2.0 are shown in Fig. 10. The robot weighs 1.37 kg and is 0.451-m high. The biped model, developed in *Autodesk Inventor*, is imported to *Msc. Visualnastran* (www.mscsoftware.com) simulation environment. The biped parameters in Table I are collected from *Msc. Visualnastran* simulation environment and used in the computation of biped dynamics.

The kinematic model of BRAIL 2.0 is shown in Fig. 2(b). The lengths and masses of the foot, shank, thigh, and torso links are d_i and m_i (with $i = 1, 2, 3, 4$), respectively. Body angles, i.e., ankle, knee, and hip angles are $\theta_b = [\theta_{b1} \ \theta_{b2} \ \theta_{b2}^T]^T$. Biped’s absolute orientation is $\theta_a = [\theta_1 \ \theta_b^T]^T$.

5.1.1. Actuators. The RX-64 motors from *Robotis, Inc.* (www.robotis.com) are used as actuators. The motors weigh 116 g and provide a maximum torque of 6.4 Nm. With two

Table I. Parameters of the biped.

Link	Length (m)	Mass (kg)	CM (m)	Inertia about CM (kg m ²)
1	$d_1 = 0.12$	$m_1 = 0.32^a$	0.085	4.56×10^{-5}
2	$d_2 = 0.1$	$m_2 = 0.13^a$	0.05	4.6×10^{-5}
3	$d_3 = 0.107$	$m_3 = 0.61^a$	0.0535	3.65×10^{-4}
4	$d_4 = 0.19$	$m_4 = 0.31$	0.17	2.88×10^{-4}

^a $m_1/m_2/m_3$: Sum of the foot/shank/thigh masses in the two legs.

Table II. Different parameters values at jumping phases.

Phase	Time (s)	θ_1 (rad)	θ_{b2} (rad)	θ_{b3} (rad)	θ_{b4} (rad)	$\dot{\theta}_1$ (rad/s)	$\dot{\theta}_{b2}$ (rad/s)	$\dot{\theta}_{b3}$ (rad/s)	$\dot{\theta}_{b4}$ (rad/s)	$x_{cm}(\theta_a)$ (m)	$y_{cm}(\theta_a)$ (m)
Take-off	0	0	2.3638	-1.5217	1.5286	0	0	0	0	0.0646	0.1155
	0.15	0.2646	1.8314	-0.5049	0.2492	0.9529	-11.2516	21.6933	-15.7940	0.0600	0.1797
Flight	0.1501	0.2646	1.8314	-0.5049	0.2492	0.9529	-11.2516	21.6933	-15.7940	0.0600	0.1797
	0.2866	0.1063	2.0276	-0.9337	0.5272	-1.9108	-2.4983	5.2413	-1.8405	0.0841	0.1585
Impact	0.2866	0.1063	2.0276	-0.9337	0.5272	-9.7475	5.0864	9.1061	-6.4239	0.0841	0.1585
Touch-down	0.2867	0.1063	2.0276	-0.9337	0.5272	-9.7475	5.0864	9.1061	-6.4239	0.0841	0.1585
	0.3003	0	2.0772	-0.8527	0.4739	-1.7766	2.4923	3.4644	-1.9522	0.0883	0.1492

actuators at each joint in sagittal plane, the maximum torque available at any joint is 12.8 Nm.

5.1.2. Controller. The motors are controlled using a CM2 controller board (www.robotis.com). The CM2 board uses an ATmega128, 16 MHz processor. The controller can be connected to the PC, using a RS232 port through which HEX code, generated from C programs, are downloaded. A unique ID is set for each actuator for the controller to communicate with them. The motors utilize RS-485 communication protocol to use the daisy chain technology.

5.2. Landing stability analysis: simulations

Simulations are done based on the parameters shown in Table I. The dynamics of the biped is computed in the MATLAB/Simulink environment. The dynamic parameters are expressed in C language code by using “c-code” command for faster computation and simulation. The control algorithms are simulated in Microsoft VC++ environment, using the C code of the biped dynamics generated by MATLAB/Simulink.

The jumping gait is divided into three phases: Take-off, flight, and touch-down. The biped’s absolute position is specified by the Cartesian coordinates of CM (x_{cm} , y_{cm}) with respect to the world coordinate frame X - Y . In the take-off phase, the foot link is in contact with the ground and $\dot{y}_{cm} > 0$. The biped is said to be in touch-down phase when the foot link is in contact with the ground and $\dot{y}_{cm} < 0$. There is no contact with the ground in flight phase. Impact occurs at the end of flight phase.

The jumping gait is generated as described in ref. [3]⁵. The control input to the three joints (ankle, knee, and hip) is formulated as output-zeroing problem, where the three joint angular positions $[\theta_{b1} \ \theta_{b2} \ \theta_{b3}]^T$ are chosen as the output functions. The initial posture of the biped considered is $\theta_a = [0 \ 2.3638 \ -1.5217 \ 1.5286]^T$ rad with zero-joint angular velocities. The joint angular positions and velocities at different phases of jumping gait are shown in Table II. We are mainly interested in the stability analysis of the touch-down phase (details of the gait generation method are available in ref. [3]). Angular positions and velocities at the beginning of the touch-down phase, $t = 0.2867$ s, indicate $\sigma_0 = -0.1620 \text{ kg m}^2 \text{ s}^{-1}$ and $\theta_{10} = 0.1063$ rad, i.e., the biped lands with foot rotated in forward direction by an 0.1063 rad with $-0.1620 \text{ kg m}^2 \text{ s}^{-1}$ angular momentum about toe. The states $x_s(t_k)$ are computed solving (9) at every

⁵ Plots of the various states during the jumping gaits are available in ref. [3].

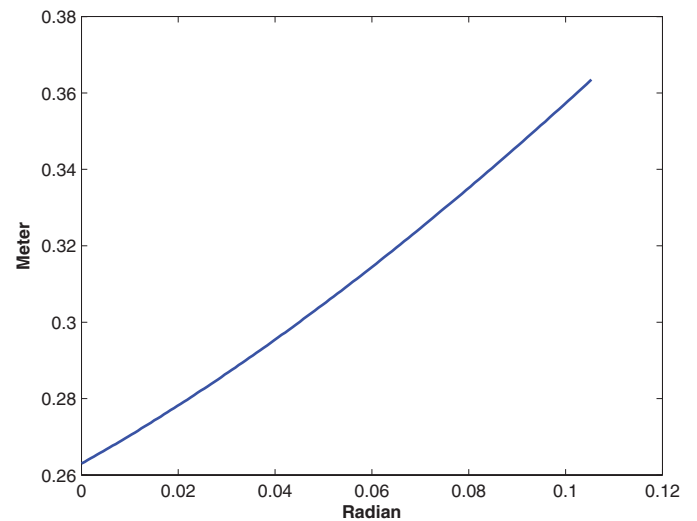


Fig. 11. $\theta_1(t_k)$ vs. $x_{RSI}(t_k)$: $\theta_{10} = 0.1063$ rad and $\sigma_0 = -0.1620 \text{ kg m}^2 \text{ s}^{-1}$.

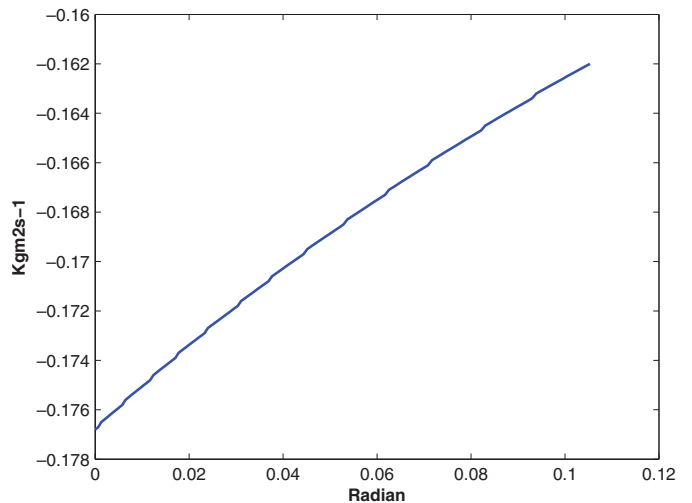


Fig. 12. $\theta_1(t_k)$ vs. $\sigma(t_k)$: $\theta_{10} = 0.1063$ rad and $\sigma_0 = -0.1620 \text{ kg m}^2 \text{ s}^{-1}$.

integration step based on fourth-order Runge–Kutta method with a fixed step size of 0.0001 s. The RSI point is computed as per (13) in every sample (i.e., integration time 0.0001 s). Figure 11 shows the plot of $\theta_1(t_k)$ versus $x_{RSI}(t_k)$. The foot link reaches $\theta_1 = 0$ plane at $t = 0.3003$ s. Figure 12 shows that the solution vector of (10) reaches $\theta_1 = 0$ with time, i.e., the biped’s landing is rotationally stable. This is also supported by Fig. 11 where it is seen that $x_{RSI f}(t_k) > 0$

Table III. RSI point computed using measured actuator positions and velocities.

t_k (s)	$\theta_1(t_k)$ (rad)	$\sigma(t_k)$ (kg m ²)	$K_1(k)$ (kg ⁻¹ m ⁻²)	$K_2(k)$ (Nm)	$K_3(k)$ (rad)	$K_4(k)$ (kg m ² s ⁻¹)	$x_{\text{RSI}}(t_k)$ (m)
0.33	0.0451	-0.1362	17.8059	2.1053	0.4667	-0.0370	0.1138
0.34	0.0250	-0.1440	17.6754	2.1159	0.4709	-0.0166	0.1323
0.35	0.0100	-0.1477	17.7723	2.1119	0.4808	-0.0031	0.1455

during landing, and according to Proposition 1, the landing should be (rotationally) stable with such locations of the RSI point⁶.

5.3. Landing stability analysis: experiment

For jumping gait realization, the actuators (Section 5.1.1) are operated in torque control mode (“endless turn mode”). The input torques to the actuators at ankle, knee, and hip are computed based on the chosen control law (i.e., output zeroing). The controller (in Section 5.1.2) reads the feedback from the actuators and computes the biped dynamics at each sampling instant. Controller sampling time is 0.01 s, i.e., controller applies the control input to the actuators each 0.01 s. $\theta_1(t_k)$ and $\sigma(t_k)$ are computed from the internal dynamics (9) (by fourth-order Runge–Kutta method with fixed step size of 0.01 s), using the measured actuator positions and velocities for $x_b(t_k)$. Thereafter, the RSI point is computed as per (13), using such measured $x_b(t_k)$ at each sampling instant.

In the experimental study, the biped lands at $t = 0.33$ s with $\theta_1(0.33s) = 0.0451$ rad and $\sigma(0.33s) = -0.1362$ kg m².³ The foot link reaches $\theta_1 = 0$ plane after two samples at $t = 0.35$ s. Various parameters during landing are shown in Table III. It is clearly seen that $x_{\text{RSI}}(t_k) > 0$ during the entire touch-down (or landing) phase, and the biped is rotationally stable during landing.

The deviations of the measured positions of the RSI points from the simulated positions mainly caused by the actuator time constant, the mismatch between actual and estimated dynamic parameters, and the difference in sampling time between simulations (0.0001 s) and experiments (0.01 s).³ However, the stability properties are identical both in simulations and experimentation. The experimental results validate the simulations.

6. Conclusion

This paper introduces novel stability concepts, rotational stability, and RSI point, which indicates the state of postural stability of a biped robot. The *rotational stability* indicates whether a biped (with foot rotation) leads to a flat-foot posture with time, and the RSI point is the point on the foot–ground contact surface, which quantifies the rotational stability of the biped. It is shown that a biped, with foot rotation, is *rotationally stable* as long as the location of the RSI point satisfies the condition (17). The stability condition (17) is

⁶ It may be noticed that the joint angular velocities are nonzero, when the biped becomes flat foot, i.e., $\theta_1(t) = 0$. The RSI point is not suitable to analyze postural stability in such flat-foot scenarios. Stability in such bipeds can be analyzed either by using ZMP/FRI/CP or by using some foot–ground compliance model, as reported in ref. [3].

then utilized to analyze the postural stability of the bipedal gaits. The applicability of the concept of rotational stability and the RSI point is illustrated by taking landing stability of jumping gait as an example.

The concepts like ZMP and FRI are not applicable for postural stability analysis in tiptoed bipeds. The concepts of *rotational stability* and *RSI point* examine the postural stability of bipeds with foot rotation (tiptoed biped). The concept of RSI point is useful to analyze the stability of biped locomotion with foot rotation. Biped locomotion is stable irrespective of the occurrence of foot rotation if the location of the RSI point satisfies the bipedal stability criterion, i.e., (17). However, the RSI point is not applicable for postural stability analysis in flat-foot postures. The concepts ZMP/FRI (for flat-foot biped) and RSI point (for tiptoed biped) are complimentary.

The RSI point can be applied for stability analysis of walking gaits and investigating periodicity aspects of various periodic bipedal gaits, such as walking, hopping, and running.

Appendix A

Proof of Lemma 1

Proof: From (12),

$$\frac{d\sigma}{d\theta_1} = \frac{K_2(k)\sin(\theta_1 - K_3(k))}{K_1(k)(\sigma - K_4(k))},$$

$$(\sigma - K_4(k))d\sigma = \frac{K_2(k)}{K_1(k)}\sin(\theta_1 - K_3(k))d\theta_1. \quad (\text{A } 1)$$

Let us define $\sigma - K_4(k) = Z$. Hence, $dZ = d\sigma$ and $\sigma_0 - K_4(k) = Z_0$. Therefore, simplifying (A 1),

$$\frac{Z_0^2}{2} = \frac{Z^2}{2} + E_\sigma(\theta_1),$$

$$Z_0^2 = Z^2 + 2E_\sigma(\theta_1), \quad (\text{A } 2)$$

where $E_\sigma(\theta_1)$ is defined as follows:

$$E_\sigma(\theta_1) = - \int_{\theta_{10}}^{\theta_1} \frac{K_2(k)}{K_1(k)} \sin(\theta_1 - K_3(k)) d\theta_1,$$

$$= \frac{K_2(k)}{K_1(k)} (\cos(\theta_1 - K_3(k)) - \cos(\theta_{10} - K_3(k))). \quad (\text{A } 3)$$

The maximum value of $E_\sigma(\theta_1)$ occurs when $\theta_1 = K_3(k)$. The corresponding maximum value is denoted by E_σ^{max} ,

which is calculated by putting $\theta_1 = K_3(k)$ in (A 3).

$$E_\sigma^{\max} = \frac{K_2(k)}{K_1(k)}(1 - \cos(\theta_{10} - K_3(k))). \quad (\text{A } 4)$$

Equation (A 2) shows that if $|Z_0| > \sqrt{2E_\sigma^{\max}}$, $\sigma = K_4(k)$ does not exist in the σ trajectory. Because $|Z_0| \neq \sqrt{2E_\sigma^{\max}}$ at $\sigma = K_4(k)$. Similarly, $|Z_0| < \sqrt{2E_\sigma^{\max}}$ indicates the existence of $\sigma = K_4(k)$ in the σ trajectory. Depending on the values of (θ_{10}, σ_0) , there can be four possible cases with $\theta_{10} > 0$ (Fig. 5).

- (1) With $K_3(k) > \theta_{10}$ and $\sigma_0 > K_4(k)$, the trajectories of (12) reach $\theta_1 = 0$ plane, if there exists $\sigma = K_4(k)$ in the σ trajectory, i.e., when $|Z_0| < \sqrt{2E_\sigma^{\max}}$ or $\sigma_0 < K_4(k) + \sqrt{2E_\sigma^{\max}}$ for $\sigma_0 > K_4(k)$.
- (2) With $K_3(k) > \theta_{10}$ and $\sigma_0 < K_4(k)$, the trajectories of (12) always reach $\theta_1 = 0$ plane.
- (3) With $K_3(k) \leq \theta_{10}$ and $\sigma_0 > K_4(k)$, the trajectories of (12) never reach $\theta_1 = 0$.
- (4) With $K_3(k) \leq \theta_{10}$ and $\sigma_0 < K_4(k)$, the trajectories of (12) reach $\theta_1 = 0$ plane, if there is no $\sigma = K_4(k)$ in the σ trajectory, i.e., when $|Z_0| > \sqrt{2E_\sigma^{\max}}$ or $\sigma_0 < K_4(k) - \sqrt{2E_\sigma^{\max}}$ for $\sigma_0 < K_4(k)$.

Cases 1 and 2 prove statement (A), while cases 3 and 4 prove statement (B).

Appendix B

Proof of Lemma 2

Proof: The x -coordinate or the ground projection of the biped's CM $x_{cm}(\theta_1, \theta_b(t_k))$ is given by (B 1).

$$x_{cm}(\theta_1, \theta_b(t_k)) = \frac{K_2(k)}{mg} \sin(K_3(k) - \theta_1). \quad (\text{B } 1)$$

Using (13) and (B 1), $x_{RSI}(t_k) > 0$ gives

$$\begin{aligned} x_{cm}(\theta_{10}, \theta_b(t_k)) - \frac{\sigma_0 - K_4(k)}{mg} \\ \times \sqrt{\frac{K_1(k)K_2(k)(1 + \cos(K_3(k) - \theta_{10}))}{2}} > 0 \\ \Rightarrow \sigma_0 < K_4(k) + \sqrt{\frac{2K_2(k)}{K_1(k)} \frac{\sin(K_3(k) - \theta_{10})}{\sqrt{1 + \cos(\theta_{10} - K_3(k))}}}. \end{aligned} \quad (\text{B } 2)$$

For the statement (A), $K_3(k) > \theta_{10}$

$$\begin{aligned} \frac{\sin(K_3(k) - \theta_{10})}{\sqrt{1 + \cos(\theta_{10} - K_3(k))}} &= \frac{\sqrt{1 - \cos^2(K_3(k) - \theta_{10})}}{\sqrt{1 + \cos(\theta_{10} - K_3(k))}} \\ &= \sqrt{1 - \cos(\theta_{10} - K_3(k))}. \end{aligned} \quad (\text{B } 3)$$

Using (B 2) and (B 3), it is seen that statement (A) is true, when $K_3(k) > \theta_{10}$ and $x_{RSI}(t_k) > 0$.

For the statement (B), $K_3(k) \leq \theta_{10}$

$$\begin{aligned} \frac{\sin(K_3(k) - \theta_{10})}{\sqrt{1 + \cos(\theta_{10} - K_3(k))}} &= -\frac{\sqrt{1 - \cos^2(\theta_{10} - K_3(k))}}{\sqrt{1 + \cos(\theta_{10} - K_3(k))}} \\ &= -\sqrt{1 - \cos(\theta_{10} - K_3(k))}. \end{aligned} \quad (\text{B } 4)$$

Using (B 2) and (B 4), it is seen that statement (B) is true, when $K_3 \leq \theta_{10}$ and $x_{RSI}(t_k) > 0$.

References

1. A. Goswami, "Postural stability of biped robots and the foot-rotation indicator (FRI) point," *Int. J. Robot. Res.* **18**(6), 523–533 (1999).
2. M. Vukobratovic and B. Borovac, "Zero-moment point—thirty five years of its life," *Int. J. Humanoid Robot.* **1**(1), 157–173 (2004).
3. D. Goswami and P. Vadakkepat, "Planar bipedal jumping gaits with stable landing," *IEEE Trans. Robot.* **25**(5), 1030–1046 (2009).
4. M. B. Popovic, A. Goswami and H. Herr, "Ground reference points in legged locomotion: Definitions, biological trajectories and control implications," *Int. J. Robot. Res.* **24**(12), 1013–1032 (2005).
5. E. R. Westervelt, J. W. Grizzle, C. Chevallereau, J. Choi and B. Morris, *Feedback Control of Dynamic Bipedal Robot Locomotion* (CRC Press, Boca Raton, 2007).
6. T. Arakawa and T. Fukuda, "Natural Motion Generation of Biped Locomotion Robot Using Hierarchical Trajectory Generation Method Consisting of GA, EP Layers," *IEEE International Conference on Robotics and Automation*, vol. 1, (1997) pp. 211–216.
7. J. J. Craig, *Introduction to Robotics: Mechanics and Control* (Addison-Wesley Longman Publishing Co., Inc. Boston, MA, 1989).
8. A. Isidori, *Nonlinear Control Systems* (Springer-Verlag, New York, 1995).
9. J. E. Slotine and W. Li, *Applied Nonlinear Control* (Prentice Hall, Englewood Cliffs, New Jersey, 1991).
10. M. W. Spong and M. Vidyasagar, *Robot Dynamic and Control* (John Wiley and Sons, New York, 1989).
11. H. K. Khalil, *Nonlinear Systems* (Prentice Hall, Portland, OR, 2001).
12. M. Vukobratović, *Biped Locomotion: Dynamics, Stability, Control and Application* (Springer-Verlag, Berlin and New York, 1990). [Online]. Available: <http://www.getcited.org/inst/144229>
13. K. Nagasaka, Y. Kuroki, S. Suzuki, Y. Itoh and J. Yamaguchi, "Integrated Motion Control for Walking, Jumping and Running on a Small Bipedal Entertainment Robot," *IEEE International Conference on Robotics and Automation*, (Apr. 26–May 1, 2004) pp. 3189–3194.
14. P. Vadakkepat, D. Goswami and C. M. Hwee, "Disturbance rejection by online ZMP compensation," *Robotica* **26**, 9–17 (2007).
15. S. N. Napoleon and M. Sampei, "Balance Control Analysis of Humanoid Robot Based on ZMP Feedback Control," *IEEE International Conference on Intelligent Robots and System*, (2002) pp. 2437–2442.
16. M. Nikkha, H. Ashrafiuon and F. Fahimi, "Robust control of underactuated bipeds using sliding modes," *Robotica* **25**(3), 367–374 (May 2007).
17. M. D. Berkemeier and R. S. Fearing, "Tracking fast inverted trajectories of the underactuated acrobot," *IEEE Trans. Robot. Autom.* **15**, 740–750 (1999).

18. C. Chevallereau, E. R. Westervelt and J. W. Grizzle, "Asymptotically stable running for a five-link, four-actuator, planar bipedal robot," *Int. J. Robot. Res.* **24**(6), 431–464 (2005).
19. E. R. Westervelt, J. W. Grizzle and D. E. Koditschek, "Hybrid zero dynamics of planar biped walkers," *IEEE Trans. Autom. Control* **48**(1), 42–56 (Jan. 2003).
20. M. H. Raibert, H. B. Brown, Jr. and M. Chepponis, "Experiments in balance with a 3D one-legged hopping-machine," *Int. J. Robot. Res.* **3**(2), 75–92 (1984).
21. Y. Hurmuzlu and D. B. Marghitu, "Rigid body collisions of planar kinematic chains with multiple contact points," *Int. J. Robot. Res.* **13**(1), 82–92 (1994).
22. D. Goswami, P. Vadakkepat and P. D. Kien, "Genetic algorithm-based optimal bipedal walking gait synthesis considering tradeoff between stability margin and speed," *Robotica* **27**, 355–365 (2009).
23. D. P. Bertsekas and I. B. Rhodes, "On the minimax reachability of target sets and target tubes," *Automatica* **7**, 233–247 (1971).